Heterogeneous mass transfer models for gas absorption in multiphase systems

Brilman, D.W.F.; Goldschmidt, M.J.V.; Versteeg, G.F.; Swaaij, W.P.M. van

Published in:
Chemical Engineering Science

DOI:
10.1016/S0009-2509(99)00491-1

PERGAMON

Chemical Engineering Science 55 (2000) 2793–2812

Chemical Engineering Science

Heterogeneous mass transfer models for gas absorption in multiphase systems

D. W. F. Brilman*, M. J. V. Goldschmidt, G. F. Versteeg, W. P. M. van Swaaij

University of Twente, Department of Chemical Engineering, PO Box 217, 7500 AE Enschede, The Netherlands

Received 15 March 1998; accepted 23 August 1999

Abstract

Heterogeneous, instationary 2-D and 3-D mass transfer models were developed to study the effect of dispersed liquid-phase droplets near the gas–liquid interface on the local gas absorption rate. It was found among other things that droplets (or particles) influence local mass transfer rates over an area exceeding largely the projection of the droplets on the gas–liquid interface. For a specific application particle–particle interaction was studied and could be described by a single parameter, depending only on the minimum interparticle distance. For gas absorption flux prediction an unit cell must be defined. The sensitivity of the absorption flux to the definition of the unit cell was investigated. Finally, a complete strategy to arrive at gas absorption flux prediction from single particle simulations has been proposed. © 2000 Elsevier Science Ltd. All rights reserved.

Keywords: Mass transfer; Heterogeneous model; Enhancement; Multiphase

1. Introduction

In three-phase reactors, gas–liquid–solid or gas–liquid–liquid, frequently the absorption rate of a (sparingly) soluble gas-phase reactant to the reaction phase is rate determining (see e.g. Beenackers & van Swaaij, 1993). The gas–liquid mass transfer rate may be enhanced significantly by the presence of a finely dispersed, liquid or solid, phase present in the bulk liquid phase. This was shown experimentally by among others Kars, Best and Drinkenburg (1979) and Alper and Deckwer (1981) for the addition of fine solid particles to a gas–liquid system. The addition of fine particles caused an enhancement of the specific gas absorption rate (per unit of driving force and interfacial area, based on the two-phase system), whereas larger particles showed almost no effect.

The increase of the specific gas absorption rate, at unit driving force and unit interfacial area, due to the presence of the dispersed phase can be characterized by an enhancement factor, E. This enhancement factor is defined as the ratio of the absorption flux in the presence of the particles (which can be solid particles or liquid droplets) to the absorption flux at the same hydrodynamic conditions and driving force for mass transfer without such particles respectively. Using this definition, possible effects of the presence of particles on the gas–liquid interfacial area and on local hydrodynamics are taken into account. For a complete and more detailed review the reader is referred to Beenackers and van Swaaij (1993).

The enhancement of the specific absorption flux due to the presence of fine particles has been explained by the so-called 'grazing'- or 'shuttle'- mechanism, see Kars et al. (1979) or Alper, Wichtendahl and Deckwer (1980). According to this shuttle-mechanism particles travel frequently between the stagnant mass transfer zone (according to the film theory) at the gas–liquid interface and the liquid bulk. Due to preferential absorption of the diffusing gas-phase component in the dispersed phase particles the concentration of this gas-phase reactant in the liquid phase near the interface will be reduced, leading to an increased absorption rate. After a certain contact time, the particle is returned to the liquid bulk where the gas-phase component is desorbed owing to the local concentration differences and the particles are regenerated. This shuttle mechanism requires that the dispersed phase particles are smaller than the stagnant mass transfer film thickness, δ_F according to the film theory. For gas absorption in aqueous media in an intensely agitated contactor, a typical value for δ_p is approximately 10–20 μm, whereas for a (laboratory) stirred cell apparatus this value is typically about a few hundred microns.

* Corresponding author. Tel.: 0031-534894479; fax: 0031-534894774.

PII: S0009-2509(99)00491-1

Nomenclature

A	area, m^2
BCG	Basic Composite Grid,
c	concentration, mol/m^3
D	diffusion coefficient, m^2/s
D_R	relative diffusion coefficient $\{=D_d/D_c\}$, dimensionless
d	characteristic particle diameter, m
d_p	particle diameter, m
d_d	drop diameter, m
E	enhancement factor, dimensionless
G	gas phase,
I	interaction parameter, dimensionless
J	mass transfer flux, mol/m^2 s
k_L	liquid side mass transfer coefficient, m/s
L	distance to the gas–liquid interface, m
m_R	relative solubility or distribution coefficient, dimensionless
N	number of particles, dimensionless
r	radial position, dimensionless
R	chemical reaction rate, mol/m^3 s
R_d, R_b	radius of droplet and bubble, respectively, m
spc	single particle cell
t	time, s
w	minimum (surface-to-surface) distance between particles, m
x	position perpendicular to gas–liquid interface, m
y	position along the gas–liquid interface, m

Greek letters

δ	mass transfer zone near interface, m
δ_p	penetration depth, m
ε_{dis}	fraction dispersed phase, dimensionless
ϕ	Hatta number, dimensionless
τ	gas–liquid contact time, s

Subscripts and superscripts

av	average value
b	bubble
bulk	at bulk liquid phase conditions
con	continuous phase
d	droplet
dis	dispersed phase
film	according to the film theory
gas	gas phase
het	heterogeneous (model)
hom	homogeneous (model)
max	maximum
p	physical absorption

Owing to a particle size distribution also in applications where the mean particle diameter is relatively large, a significant enhancement of the gas absorption rate may be observed. This was confirmed experimentally by Tinge and Drinkenburg (1995), who added very fine particles to a slurry consisting already of larger ones and found that the enhancement of gas absorption to be similar to the enhancement of the gas absorption rate due to the addition of only the same amount of fine particles to a clear liquid. Such size distributions will certainly occur in case of gas absorption (or solids dissolution) in a liquid–liquid dispersion. Nishikawa et al. (1994) have shown for liquid–liquid systems that the effect of aeration is a broadening of the droplet size distribution, i.e. more fine droplets. This implies that especially for gas–liquid–liquid systems enhancement of gas absorption can be expected when, of course, the solubility of the diffusing component in the dispersed liquid phase exceeds the solubility in the continuous liquid phase.

Experimentally, the gas absorption enhancement phenomenon in multiphase systems was frequently studied and a summary of relevant studies is given in Table 1. Three types of (reaction) systems have been studied experimentally; physical absorption experiments, systems with a first-order reaction for the diffusing component in the continuous phase and one for a first-order reaction in the dispersed phase. No experimental study concerning the influence of an additional second liquid phase on the selectivity for multi-reaction systems has been found in literature.

All presented experiments show that mass transfer and chemical reaction in mass transfer limited gas–liquid systems can be significantly enhanced by the addition of a second dispersed liquid phase with a good solubility ($m_R \geqslant 10$) of the solute. Enhancement factors up to 26 have been found experimentally, though usually the enhancement factor E is within the range 1–5. Some typical experimental results of the enhancement factor vs. dispersed liquid-phase hold up, as observed in G–L–L systems, are shown in Fig. 1. Note that these results are all obtained using labscale equipment.

In order to elucidate and/or describe the enhancement effect many theoretical models were developed. These can be categorized by using the model characterizations 'stationary' or 'instationary' models and '(pseudo-) homogeneous' models or 'heterogeneous' models. For the heterogeneous models a subdivision in one-dimensional, two-dimensional and three-dimensional models can be made, see Table 2. In Table 3 the models presented in literature are summarized in more detail.

Table 1
Overview of experimental work on gas absorption enhancement for G–L–L systems and for some other systems

Authors	System type	System	Apparatus	Characteristics	Geometric sizes
Mehra and Sharma (1985); Mehra, Pandit and Sharma (1988-II)	G–L–L	Absorption of isobutylene, butene-1 and propylene in emulsions of chlorobenzene in aqueous solutions of sulphuric acid	Stirred cell	$\phi = 1$–15 $\varepsilon_{dis} = 0.02$–0.30 $E = 1.5$–26 m_R isobutene: 1617 1-Butene: 2014 Propylene: 396	$d_d = 1$–$12\ \mu m$ $\langle d_d \rangle \approx 2\ \mu m$ $\delta_p \approx 100\ \mu m$
Bruining, Joosten, Beenackers and Hofman (1986)	G–L–L	Oxygen absorption into emulsions of hexadecane in sodium sulphate	Stirred cell	$\phi \approx 0.2$ $\varepsilon_{dis} = 0.01$–0.08 $E = 1$–1.4 $m_R = 11.6$	$d_d \leqslant 10\ \mu m$ $\delta_p \approx 23.5\ \mu m$
Littel et al. (1994)	G–L–L	Physical absorption of CO_2 and propylene into toluene/water emulsions	Stirred cell Laminar film	$\varepsilon_{dis} = 0.01$–0.39 $E = 1$–4.1 m_R: $CO_2 = 2.85$ Propylene $= 103$	$d_d \leqslant 3\ \mu m$ $\delta_{p,st.cell} \approx 300\ \mu m$ $\delta_{p,lam.film} \approx 65\ \mu m$
Venugopal and Mehra (1994)	G–L–L	Absorption of CO_2 into emulsions of aqueous sodium hydroxide in 2-ethyl hexanol	Stirred cell	$\phi \approx 6.4$ $\varepsilon_{dis} = 0.05$–0.2 $E = 2.4$–3.8 m_R $CO_2 = 1.9$	$d_d = 5$–$8\ \mu m$ $\delta_p \approx 400\ \mu m$
Van Ede et al. (1995)	G–L–L	Oxygen absorption into emulsions of octene in sodium sulphate	Stirred cell	$\phi \approx 0.2$ $\varepsilon_{dis} = 0.05$–0.5 $E = 1.5$–3.7 $m_R \approx 18$	$d_d = 22\ \mu m$ $\delta_p \approx 25\ \mu m$
Kars et al. (1979)	G–L–S	Absorption of propane in a slurry of active carbon in water	Stirred cell	$E \approx 1.3$ $\varepsilon_{dis} = 0.5$–5 wt%	$d_d = 30$–$530\ \mu m$ $\delta_p \approx 20\ \mu m$
Alper et al. (1980)	G–L–S	Absorption of CO_2 in an aqueous carbonate-bicarbonate buffer with carbonic anhydrase supp. on oxirane-acrylic beads	Stirred cell	$\phi \approx 0.32$ $\varepsilon_{dis} = 0$–0.5 wt% $E = 1.2$–3.5	$d_d = 1$–$20\ \mu m$ $\delta_p \approx 37.5\ \mu m$
Pal, Sharma and Juvekar (1982)	G–L–S	Oxidation of aqueous sodium sulphite in the presence of activated carbon	Stirred cell	$\phi \approx 2.7$ $\varepsilon_{dis} = 0.01$–2.0 wt% $E = 1.4$–1.9	$d_d = 1.7$ and $4.3\ \mu m$ $\delta_p \approx 56\ \mu m$
Mehra et al. (1988)	S–L–L	Alkaline hydrolysis of solid esters in emulsions of chlorobenzene in aqueous solution of potassium hydroxide	Stirred cell	$\phi = 0.4$–1.9 $\varepsilon_{dis} = 0.005$–$0.20$ $E = 1.7$–12 m_R: $PB = 5170$ 2,4-DCPB $= 8890$ DCPB $= 7085$	$d_{2,4\text{-DCPB}} = 235\ \mu m$ $d_{DCPB} = 195\ \mu m$ $d_{PB} = 120\ \mu m$ $d_d = 1$–$12\ \mu m$ $\langle d_d \rangle \approx 3$–$4\ \mu m$ $\delta_p \approx 240\ \mu m$
Tinge, Mencke and Drinkenburg (1987)	G–L–S	Absorption of a mixture of propane and ethene in a slurry of activated carbon in water	Stirred cell	$\varepsilon_{dis} = 0.01$ $m_{R,\ ethene} = 65$ $m_{R,\ propane} = 1500$	$d_d = 40$–$63\ \mu m$ and 500–$630\ \mu m$ $\delta_p < 100\ \mu m$
Rols, Condoret, Fonade and Goma (1990)	G–L–L–S	Oxygen absorption into emulsions of *n*-dodecane and perfluoro-carbon in water, in a culture of aerobacter aerogenes	Fermentation broth	$\varepsilon_{dis} = 0.02$–0.34 $E = 1.1$–3.5 $m_{R,\ n\text{-dodecane}} = 7.7$ $m_{R,perfluoroc.} = 17$	$d_{d,\ solids} = 0.5$–$5\ \mu m$ $d_{d,liquid} = 0.5$–$50\ \mu m$ $d_b = 500$–$5000\ \mu m$
Junker et al. (1989-I)	G–L–L–S	Oxygen absorption in aqueous/perfluorocarbon fermentation systems	Fermentation broth	$\varepsilon_{dis} = 0.1$–0.95 $E = 5$–10 $m_{R,perfluoroc.} = 22$	$d_d = 50$–$100\ \mu m$ $d_b = 300\ \mu m$ $\delta_p = 15\ \mu m$
Van der Meer, Beenackers, Burghard, Mulder and Fok et al. (1992)	G–L–L–S	Oxygen absorption into emulsions of *n*-octane in water, in culture of pseud. olevorans	Fermentation broth	$\varepsilon_{dis} = 0.05$–0.11 $E = 1.1$–1.6	$d_d = 0.5\ \mu m$ $\delta_p = 5\ \mu m$

The advantage of the homogeneous models is their numerical simplicity (for simple cases they can even be solved analytically) and short computation times. For these homogeneous models the following assumptions are generally made.

- the dispersed phase droplets are very small with respect to the mass transfer film thickness according to the film theory,
- the dispersed phase (a continuum) is homogeneously distributed throughout the continuous phase,
- there is no direct gas-dispersed phase contact,
- transport occurs only through the continuous phase,
- mass transfer resistances within the dispersed phase are neglected.

Clearly, some of these assumptions are questionable. The results obtained with these models, however, do predict

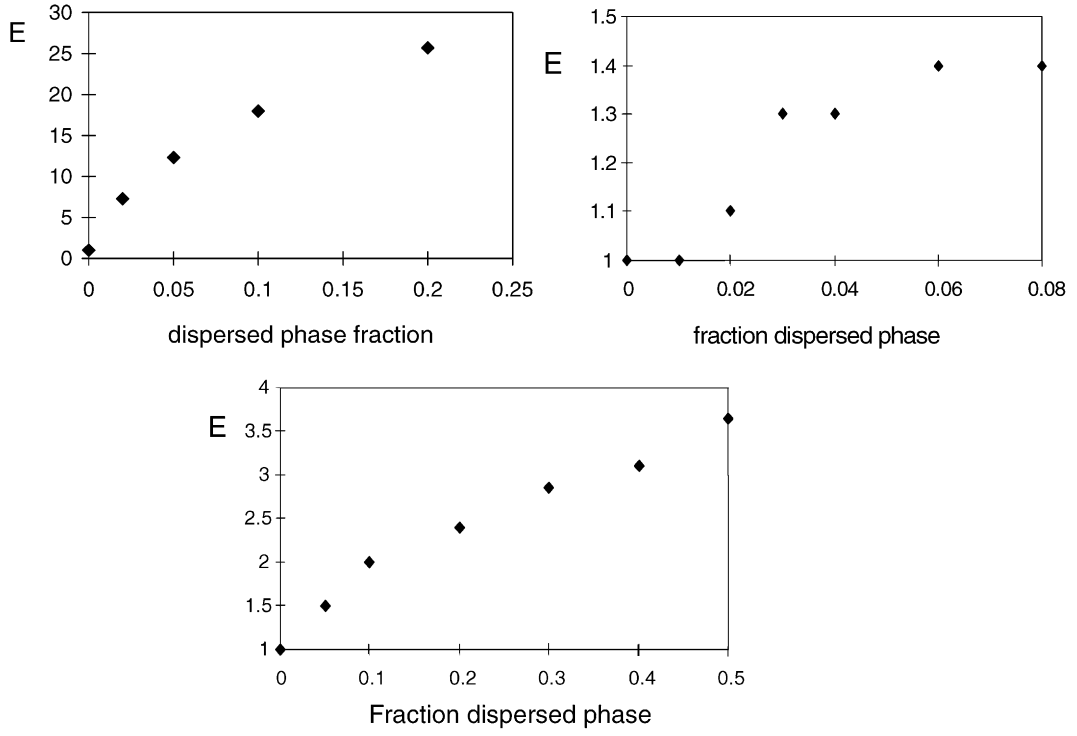

Fig. 1. Observed enhancement factors at increasing dispersed phase hold-up for G–L–L systems. a: Enhancement of butene-1 absorption in chlorobenzene/water emulsions (Mehra 1985, 1988). b: Enhancement of oxygen absorption in hexadecane/sodium sulphate emulsions (Bruining et al., 1986). c: Enhancement of oxygen absorption in octene/water + sulphate emulsion (Van Ede et al., 1995).

Table 2
Classification of models

	Steady state models	Instationary models
Homogeneous models	Mehra and Sharma (1985)	Bruining et al. (1986)
		Mehra (1988)
		Littel et al. (1994)
		Van Ede et al. (1995)
		Nagy and Moser (1995)
Heterogeneous models	3-D Holstvoogd et al. (1988)	1-D Junker et al. (1990a,b)
	3-D Karve and Juvekar (1990)	Vinke (1992)
		Nagy (1995)
		Brilman (1998)
		2-D Lin et al. (1999)
		2-D (This work)
		3-D (This work)

the trend of the enhancement factor with changing operating conditions as the gas–liquid contact time, the relative solubility and the dispersed phase fraction qualitatively reasonably well.

Since the quantitative agreement of the homogeneous models with the results of the experimental studies is not completely satisfactory, several authors even adapted these models to fit their experimental data better. Van Ede, Van Houten and Beenackers (1995) assumed the dispersed phase fraction in the mass transfer zone to increase with the distance to the gas–liquid interface from a zero fraction at the gas–liquid interface to the bulk phase holdup. Diffusion in the droplet phase was added in this model, but this seems rather unrealistic considering the discontinuous character of the dispersed phase. Littel, Versteeg and Swaaij (1994) on the contrary, assumed in their modeling a thin layer of the dispersed phase at the gas–liquid interface to account for the large differences between the experimentally observed enhancement factors using the stirred cell apparatus and the ones calculated with the homogeneous model. By using a laminar, falling film apparatus Littel et al. (1994) were able to minimize the effect of gravity, i.e. to prohibit settling of the dispersed phase. In the latter set of experiments the (homogeneous) model predictions were already much better in agreement with experimentally determined absorption fluxes.

Heterogeneous mass transfer models, taking into account the local geometry at the gas–liquid interface, will increase the level of understanding of the mass transfer enhancement phenomena at the gas–liquid interface. For gas–liquid–liquid systems one-dimensional, instationary, heterogeneous mass transfer models for one particle in the penetration film were developed by Junker, Wang and Hatton (1990a) and Nagy (1995). Their models could

Table 3
Overview of mass transfer models for microphase systems

Authors	Characteristics	Application	Model representation
Mehra and Sharma (1985)	Film model Stationary model	G–L–S	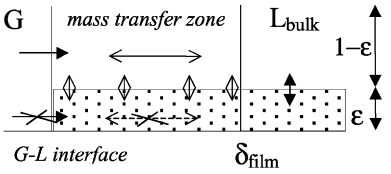
Bruining et al. (1986)	Penetration model $E = \sqrt{1 + \varepsilon(m_R - 1)}$	G–L–L Physical absorption	
Holstvoogd et al. (1988)	Unit cell approach N (= 1,2,3) particles in a row stationary model instantaneous surface reaction	G–L–S effect of particle -geometry	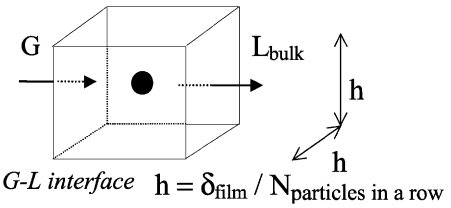
Mehra (1988)	Surface renewal model instationary, reaction in both phases poss.	G–L–L 1st order reaction effect ε, a_{LL}	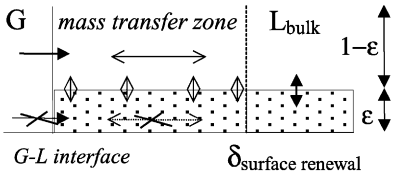
Saraph and Mehra (1994)	See Mehra (1988)	G–L–S, precipitation ('auto-catalytic effect')	[see Mehra (1988)]
Venugopal and Mehra (1994)	See Mehra (1988)	G-L-L, w/o emulsion, fast reaction in the aqueous phase	[see Mehra (1988)]
Junker et al. (1989)	Penetration model 2 'plates' in series (1D)	G–L–L physical absorption + 0th order reaction o/w ‖ w/o transition	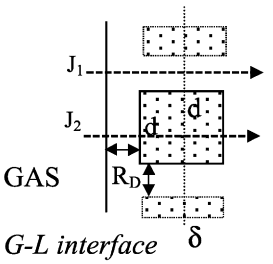
Karve and Juvekar (1990)	Unit cell approach stationary model instantaneous surface reaction equal probability for particle position for $d_p/2 \leqslant M(x) \leqslant \delta - d_p/2$	G–L–S interparticle effect 1st order reaction effect ε, d_p	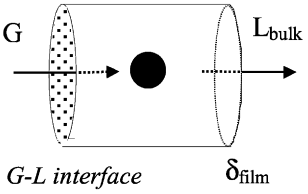
Rols et al. (1991)	Macrosc. absorption model parallel transport via direct gas-dispersed phase contact collision/break-up proposed for G–L–L systems	$(k_La)_{G\to Lc} + (k_La)_{G\to Ld}$	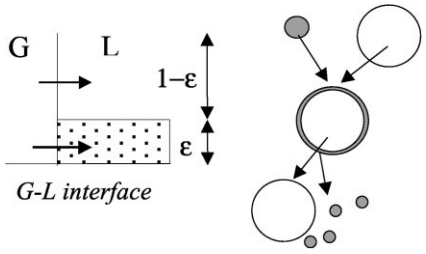

Table 3 (*continued*)

Authors	Characteristics	Application	Model representation
Vinke et al. (1992)	Stationary film model for solid particles in the film Parallel transport covered- and uncovered surface particles represented by a slab (at $x = d_p/4 - d_p/2$) (1D heterogeneous)	G–L–S effect of particle adsorption capacity and adhering properties	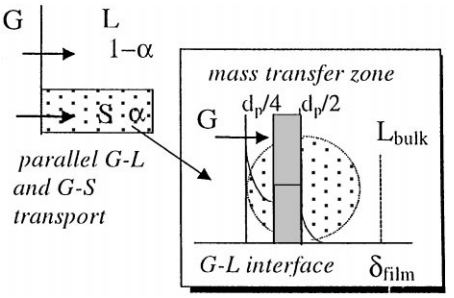
Littel et al. (1994)	Penetration model instationary	G–L–L idea of microscopic phase separation physical absorption effect $\varepsilon_{interface} > \varepsilon_{bulk}$	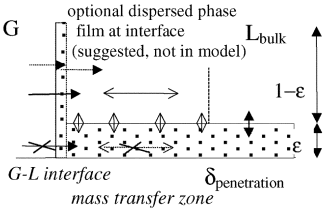
Nagy and Moser (1995)	Film-penetration theory ('pseudo'-hom. model) effect of L-L mass transfer and mass transfer inside drops	G–L–L 0th-, 1st-order reaction	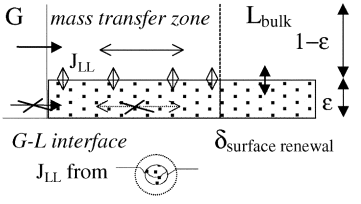
Nagy (1995)	Film-penetration model (2 parameter model) 1D heterogeneous	G–L–L Physical absorption 0th-, 1st- order reaction	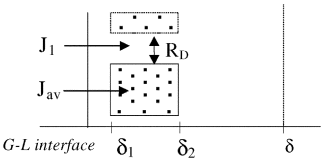
Van Ede et al. (1995)	Dispersed phase holdup varies with distance to G/L interface	Physical absorption 1st-order reaction	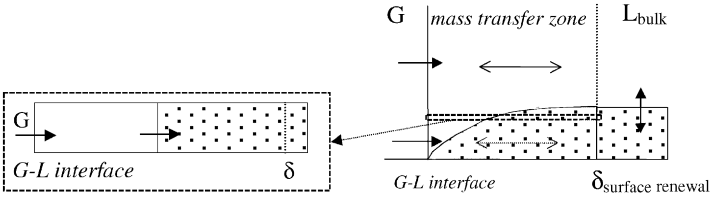
Brilman (this work)	Instationary heterogeneous models: 1-D, 2-D and 3-D • introduction *foreland* • effect geometry factors (d_p, L, R_b/R_d) • particle interaction • effect of choice of unit cell		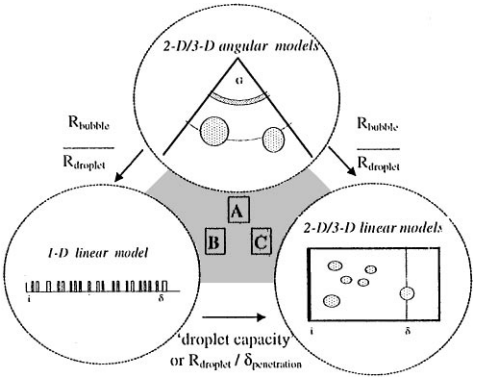

be solved analytically for some specific cases as, e.g. physical absorption. These were developed to describe mass transfer (+ reaction) in systems in which the dispersed phase drops are of the same size as the penetration film thickness. However, especially in these cases the sphericity of the gas bubble as well as the sphericity of the droplet may influence significantly the mass transfer rates. A numerical 1-D model, capable of handling multiple particles and more complex situations was presented by Brilman et al. (1998).

For gas–liquid–solid systems some *stationary* 3-D heterogeneous models were developed by Holstvoogd, van Swaaij and Dierendonck (1988) and Karve and Juvekar (1990). In both studies an unit cell approach was used, containing one single particle in the cell. The results of the heterogeneous models by Holstvoogd et al. (1988), Karve et al. (1990) and the 1-D models of Nagy (1995) and Brilman (1998) have shown that enhancement of gas–liquid mass transfer is dominated by the first particles near the gas–liquid interface. Further, it was shown by Holstvoogd et al. (1988) that local geometry strongly influences the enhancement factors found, indicating that a homogeneous description of the dispersed phase is not appropriate.

2. Heterogeneous mass transfer models

From the short overview given above it is concluded that *instationary three dimensional* mass transfer models are desired to investigate the importance of the geometrical factors involved in these multiple-phase systems. It is necessary that the models to be developed are instationary in order to incorporate the effect of 'saturation' of the dispersed phase particles during the gas–liquid contact time. Next to these effects of near interface geometry also particle–particle interaction and the translation of modeling results to actual absorption flux prediction will be discussed in this work.

For the development of a three-dimensional model in which local geometry is taken into account the characteristic geometrical size (or -) ratios should be measured or estimated. In general, bubbles are large with respect to the droplet size and the penetration film thickness. In these cases the interface can be regarded as a plane (in this work called 'linear' or 'planar' models). For strong ionic solutions, at high power inputs in agitated systems or for a dissolving solid in a liquid–liquid system this is not necessarily the case and the bubble sphericity or solid particle size needs to be taken into account. This latter effect is taken into account in the so-called 'angular models', presented in this work. Therefore, a complete set of models has been developed and is presented schemetically in Fig. 2.

Depending on the geometrical size ratio $R_{\text{bubble}}/R_{\text{droplet}}$ and the relative 'droplet absorption capacity' one of these models will be most appropriate. Model A takes both the

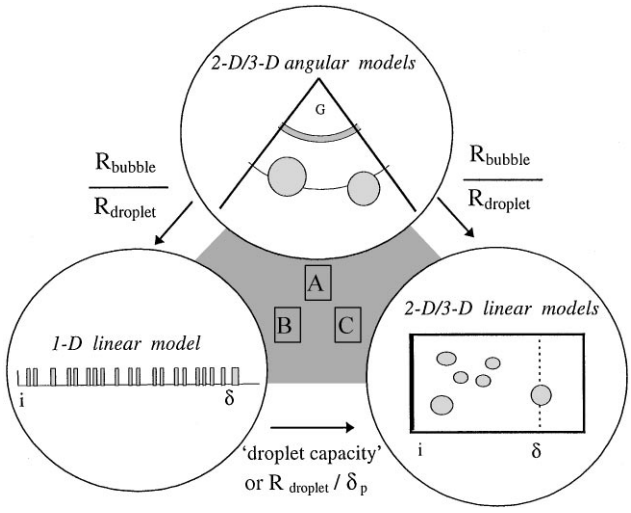

Fig. 2. Set of heterogeneous, instationary mass transfer models.

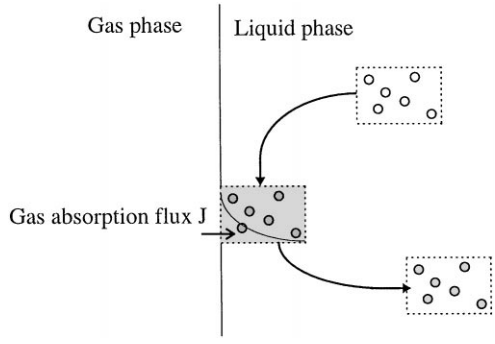

Fig. 3. Gas absorption (in a multiphase system) according to the penetration theory.

sphericity of the gas bubble and the drop into account. If the bubble size is much larger than the penetration film thickness the sphericity of the gas–liquid interface can be neglected. For very small particles with a low capacity the one-dimensional model B may be found convenient and sufficient accurate, whereas for somewhat larger particles or particles with a higher capacity for the diffusing solute model C is most appropriate. In theory, in all the models described in Fig. 2 the number, position and size of the drops, etc. can be chosen arbitrarily.

For modeling mass transfer in multiple-phase systems it is required to adopt a fundamental mass transfer model like the Higbie penetration model or the film model. The Higbie model is applied in the present study, thus assuming that a package of the bulk liquid phase, including the dispersion droplets present within the package, is transported to the gas–liquid interface and remains there for a certain contact time τ, before returning to the liquid phase bulk. Additionally, it is assumed that the position and distribution of the dispersed phase droplets within the package remains unchanged. This is represented schematically in Fig. 3.

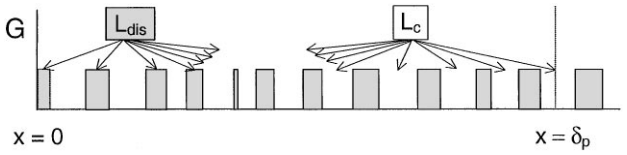

Fig. 4. The one-dimensional, instationary, multi-particle model.

A complication for the practical applicability of the heterogeneous models is the comparison of the modeling results for a particular situation with experimentally observed absorption rates. Since, in principal, an infinite number of distributions of the dispersed phase drops throughout the penetration film (liquid phase) is possible, one needs to choose either a representative 'average' configuration or use a statistical averaging technique. Since it was shown (Brilman et al., 1998) with the one-dimensional model that among others the distance of the first droplet to the gas–liquid interface has a major influence on the mass transfer enhancement, this aspect requires special attention. For 2-D and 3-D models the situation is even more complicated since particle–particle interactions are much more complex. After discussing the results for simulations with a single dispersed phase particle, effects of particle–particle interaction will be investigated using 2-D multi-particle simulations. With these results, effects of different particle configurations in a liquid package (or unit cell) can be calculated.

2.1. The one-dimensional model

In Fig. 4 a graphical representation of the one-dimensional model is given. In Fig. 4 the gas phase is on the left hand side, L_c represents the continuous liquid phase and L_{dis} the dispersed liquid-phase droplets. The parameter δ_p is the penetration film thickness, as estimated by Higbie's penetration theory for absorption in the continuous phase in the absence of the dispersed phase. The actual penetration depth will, in general, be less than δ_p due to the larger absorption capacity of the dispersed phase droplets.

The equations describing diffusion of the gas-phase solute in the stagnant continuous liquid phase and inside the dispersed phase (and chemical reaction if applicable) were solved numerically. The number of particles as well as their sizes, positions and composition can be varied arbitrarily. For more details on the model the reader is referred to Brilman et al. (1998).

2.2. Two- and three dimensional models

In Fig. 5 a typical representation of a two- or three-dimensional model is given. In this figure the gas bubble is surrounded by a larger number of droplets. In this study both the gas bubble and the droplets are considered to be spherical. The partial differential equations

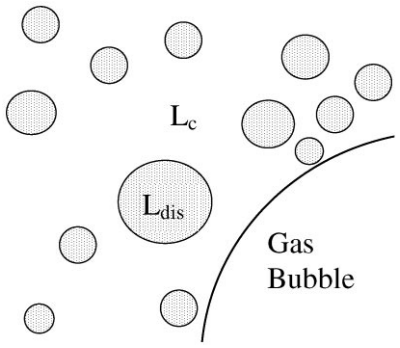

Fig. 5. Two dimensional slice of a gas–liquid–liquid system.

describing diffusion with chemical reaction in such heterogeneous media can only be solved numerically. This requires the diffusion field to be covered by a computational grid on which the partial differential equations can be solved using a finite difference approximation.

The complex geometry of the heterogeneous medium is difficult to describe using a single global grid. In this work, a composite grid, consisting of simpler component grids, suitably chosen to describe a particular subdomain and overlapping where they meet, is chosen to solve this problem. This is illustrated for the situation of one dispersed phase droplet located near the gas–liquid interface. For the 2-D and 3-D linear models (type C), the *base composite grid* (BCG) used for solving the equations is represented by the x–y plane in Fig. 6. More details on this *overlapping grid technique* are given by Chesshire and Henshaw (1994).

In Fig. 6a the geometry of the BCG for which the equations are solved is represented. The equations for the 2-D models assume no variation in the z-direction, perpendicular to the x–y plane. The 3-D single particle models use the same BCG. However, now the three-dimensional transport equations are solved. A large reduction of computational effort is hereby achieved by using the rotational symmetry around the line through the middle of the droplet, perpendicular to the gas–liquid interface.

The composition of the composite overlapping grids of Fig. 6 is clearly demonstrated in Fig. 7. The '*outer annulus*' grid enables a numerically smooth overlap from the diffusion field around the droplet with the continuous phase diffusion field. The inner radius of the *outer annulus* grid and the outer radius of the inner annulus grid join precisely and constitute the phase boundary. At this phase boundary a user-defined boundary condition is implemented, accounting for continuity of fluxes and the instantaneous equilibrium distribution of the diffusing species between both phases at the interface (see Eqs. (1a) and (1b). A small square grid inside the drop is required to avoid very small grid sizes and a singularity at the center of the inner annulus.

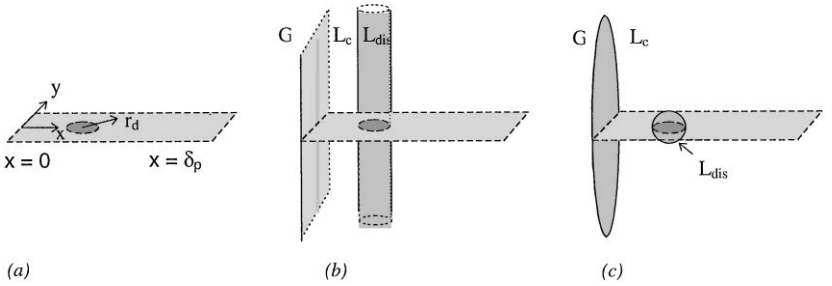

Fig. 6. Transformation of the two-dimensional plane on which the mass balances for the 2-D and 3-D linear, heterogeneous models are solved into the three-dimensional situation that these equations represent. (a) Geometry of a grid on which the model equations are solved, (b) 3-D geometry as described by the equations of the 2-D linear model, (c) 3-D geometry described by the equations of the 3-D linear model.

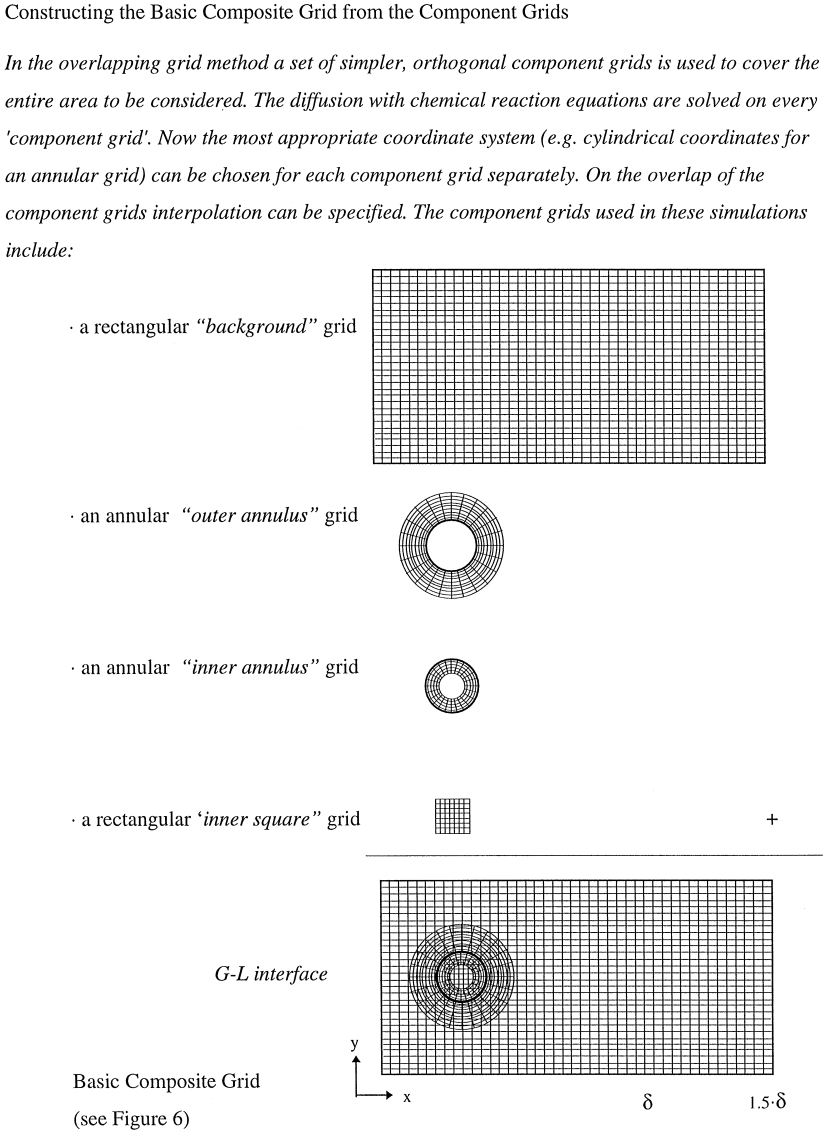

Fig. 7. Construction of the basic composite (overlapping) grid from the component grids.

The model equations for the 2-D and 3-D models are listed in Table 4. In all these equation R_{con} (or R_{dis}) is the source term due to chemical reaction. This term causes coupling of the mass balance of solute A to the mass balances of other component in case of multi-component reactions. The mass transfer resistance in the gas phase is neglected in this work.

The angular models (type A) differ from the linear models (type C) only via the *background*-grid. For the A-type models the background is chosen to be a fraction ($\approx 1/6$) of an annular grid. The equations describing diffusion with chemical reaction for the other component grids remain unchanged.

From Table 4c it can be noted that boundary conditions at overlapping component grids do not need to be specified. The continuity of the concentration profile and the conservation of mass is accounted for by the interpolation and overlap algorithms within the *Overture* software package (Los Alamos Nat. Lab., USA). At the droplet surface the inner and outer annulus component grids do not overlap, but join precisely. Here, the boundary conditions need to be specified to ensure the continuity of fluxes and to account for the distribution of the solute between both liquid phases. The equilibrium at the interface is assumed to be instantaneously fast.

$$r = R_d$$

$$C_{dis} = m_R C_{con}, \tag{1a}$$

$$\left[-D_{dis} \frac{\partial C_{dis}}{\partial r} = -D_{con} \frac{\partial C_{con}}{\partial r} \right]_{r=R_d}. \tag{1b}$$

The result of the models described above consists of a concentration profile for the diffusing component(s) in the diffusion field (at every gridpoint) for both the continuous and the dispersed phase. From the model the time-dependent specific rate of absorption per unit time and unit of gas–liquid interface, $\varphi(t)$ in [mol/m^2 s], and the average specific rate of absorption over the gas–liquid contact time, $\varphi_{av}(\tau)$ in [mol/m^2 s], are obtained at every y-position at the gas–liquid interface. The local enhancement factor $E(y,t)$ is defined by the ratio of these fluxes to their equivalent for gas absorption under identical conditions without the presence of a dispersed phase:

$$E(y,t) = \frac{\varphi(y,t)}{\sqrt{\frac{D_c}{\pi t}}}, \tag{2a}$$

$$E_{av}(y,\tau) = \frac{\varphi_{av}(y,\tau)}{2\sqrt{\frac{D_c}{\pi \tau}}}. \tag{2b}$$

The enhancement factors $E(y)$ mentioned refer always to the contact time-averaged enhancement factor $E_{av}(y,\tau)$, unless mentioned otherwise. In the simulations the depth of the diffusion field was taken 1.5 times the penetration depth of the diffusing gas-phase component ($\delta_{pen} = 2\sqrt{\pi D_c \tau}$), thus sufficiently large to assure that the concentration profile does not reach to the end of the diffusion field. The model was validated against analytical solutions for physical absorption and for absorption accompanied by a homogeneous first-order chemical reaction in the continuous phase for situations without particles.

From these test cases it is concluded that the concentrations and fluxes calculated on overlapping grids are usually calculated within 1% deviation. Convergency orders in time- and space stepsize are consistent with the Euler explicit finite difference formula used to approximate the partial differential equations on the component grids. Extrapolation to infinitely small step sizes yielded deviations from the analytical solutions of less than 0.03% in the test cases.

3. Results of simulations with one dispersed phase particle

For the single particle simulations values for the various physico-chemical parameters were taken from the experimental study of Littel et al. (1994) were chosen as default values, see Table 5. A typical single particle model simulation result is given in Fig. 8. The enhancement factor not only varies with the position along the gas–liquid interface, but also changes significantly with time (see e.g. Fig. 9c). A maximum is observed due to counteracting effects. The initial increase of $E(y,t)$ with time is due to the fact that the propagating concentration profile needs to reach the droplet, before its influence will become noticeable.

However, as time propagates, the droplet will get 'saturated' with the diffusing solute. The local decrease of its concentration in the continuous phase near the gas–liquid interface will diminish, and with this the local enhancement factors will decrease, ultimately leading to $E(y,t) = 1$ at every y-position. Another important aspect which can be recognized from Fig. 8 is the interfacial area over which the influence of the mass transfer enhancement is noticeable. In this work, it is proposed to call this the 'foreland' of the droplet.

For the single droplet case the influence of several process parameters was studied, and especially the distance of the front of the particle to the gas–liquid interface, the droplet diameter and the relative solubility m_R were varied. Examples of results are given in Fig. 9a–e for 2-D simulations. The default parameter values used are given in Table 5.

Fig. 9c shows clearly that the width of the foreland changes in time and will depend on droplet diameter, relative solubility and the continuous phase diffusion

Table 4
Mass balances and boundary conditions for the 2-D and 3-D heterogeneous mass transfer models

(a) 2-D models; Instationary mass balances for diffusing gas phase component A

2D models	Instationary mass balances
Continuous phase (rectangular '*Background*')	$\frac{\partial c_{con}(x,y,t)}{\partial t} = D_{con}\left(\frac{\partial^2 c_{con}(x,y,t)}{\partial x^2} + \frac{\partial^2 c_{con}(x,y,t)}{\partial y^2}\right) + R_{con}$
Continuous phase[a] (angular '*Background*')	$\frac{\partial c_{con}(r_b,\theta_b,t)}{\partial t} = D_{con}\left(\frac{1}{r_b}\frac{\partial}{\partial r_b}\left(r_b\frac{\partial c_{con}(r_b,\theta_b,t)}{\partial r_b}\right) + \frac{1}{r_b^2}\frac{\partial^2 c_{con}(r_b,\theta_b,t)}{\partial \theta_b^2}\right) + R_{con}$
Continuous phase around dispersed phase droplet[b] ('*outer annulus*')	$\frac{\partial c_{con}(r_d,\theta_d,t)}{\partial t} = D_{con}\left(\frac{1}{r_d}\frac{\partial}{\partial r_d}\left(r_d\frac{\partial c_{con}(r_d,\theta_d,t)}{\partial r_d}\right) + \frac{1}{r_d^2}\frac{\partial^2 c_{con}(r_d,\theta_d,t)}{\partial \theta_d^2}\right) + R_{con}$
Dispersed phase[b] ('*inner annulus*')	$\frac{\partial c_{dis}(r_d,\theta_d,t)}{\partial t} = D_{dis}\left(\frac{1}{r_d}\frac{\partial}{\partial r_d}\left(r_d\frac{\partial c_{dis}(r_d,\theta_d,t)}{\partial r_d}\right) + \frac{1}{r_d^2}\frac{\partial^2 c_{dis}(r_d,\theta_d,t)}{\partial \theta_d^2}\right) + R_{dis}$
Dispersed phase[b] ('*inner square*')	$\frac{\partial c_{dis}(x,y,t)}{\partial t} = D_{dis}\left(\frac{\partial^2 c_{dis}(x,y,t)}{\partial x^2} + \frac{\partial^2 c_{dis}(x,y,t)}{\partial y^2}\right) + R_{dis}$

(b) 3-D models; Instationary mass balances for diffusing gas phase component A

3D models	Instationary mass balances
Continuous phase (rectangular '*Background*')	$\frac{\partial c_{con}(x,y,t)}{\partial t} = D_{con}\left(\frac{\partial^2 c_{con}(x,y,t)}{\partial x^2} + \frac{1}{y}\frac{\partial}{\partial y}\left(y\frac{\partial c_{con}(x,y,t)}{\partial y}\right)\right) + R_{con}$
Continuous phase[a] (angular '*Background*')	$\frac{\partial c_{con}(r_b,\theta_b,t)}{\partial t} = D_{con}\left(\frac{1}{r_b^2}\frac{\partial}{\partial r_b}\left(r_b^2\frac{\partial c_{con}(r_b,\theta_b,t)}{\partial r_b}\right) + \frac{1}{r_b^2\sin\theta_b}\frac{\partial}{\partial c_{con}}\left(\sin\theta_b\frac{\partial^2 c_{con}(r_b,\theta_b,t)}{\partial \theta_d^2}\right)\right) + R_{con}$
Continuous phase around dispersed phase droplet[b] ('*outer annulus*')	$\frac{\partial c_{con}(r_d,\theta_d,t)}{\partial t} = D_{con}\left(\frac{1}{r_d^2}\frac{\partial}{\partial r_d}\left(r_d^2\frac{\partial c_{con}(r_d,\theta_d,t)}{\partial r_d}\right) + \frac{1}{r_d^2\sin\theta_d}\frac{\partial}{\partial \theta_d}\left(\sin\theta_d\frac{\partial c_{con}(r_d,\theta_d,t)}{\partial \theta_d}\right)\right) + R_{con}$
Dispersed phase[b] ('*inner annulus*')	$\frac{\partial c_{dis}(r_d,\theta_d,t)}{\partial t} = D_{dis}\left(\frac{1}{r_d^2}\frac{\partial}{\partial r_d}\left(r_d^2\frac{\partial c_{dis}(r_d,\theta_d,t)}{\partial r_d}\right) + \frac{1}{r_d^2\sin\theta_d}\frac{\partial}{\partial c_{dis}}\left(\sin\theta_d\frac{\partial^2 c_{dis}(r_d,\theta_d,t)}{\partial \theta_d^2}\right)\right) + R_{dis}$
Dispersed phase[b] ('*inner square*')	$\frac{\partial c_{dis}(r_d,\theta_d,t)}{\partial t} = D_{dis}\left(\frac{1}{r_d^2}\frac{\partial}{\partial r_d}\left(r_d^2\frac{\partial c_{dis}(r_d,\theta_d,t)}{\partial r_d}\right) + \frac{1}{r_d^2\sin\theta_d}\frac{\partial}{\partial c_{dis}}\left(\sin\theta_d\frac{\partial^2 c_{dis}(r_d,\theta_d,t)}{\partial \theta_d^2}\right)\right) + R_{dis}$

(c) 2-D and 3-D models; Initial and boundary conditions[c]

2D + 3D models				
Continuous phase (rectangular '*Background*')	IC	$t = 0$	$x \geqslant 0$	$c_{con} = 0$ (or $c_{con} = c_{con,bulk}$)
	BC	$t > 0$	$x = 0$	$c_{con} = c_{gas} M_{gl}$
			$x \to \infty$	$c_{con} \to 0$ (or $c_{con} \to c_{con,bulk}$)
Continuous phase (angular '*Background*')	IC	$t = 0$	$r_b \geqslant R_b$	$c_{con} = 0$ (or $c_{con} = c_{con,bulk}$)
	BC	$t > 0$	$r_b = R_b$	$c_{con} = c_{gas} m_{GL}$
			$r_b \infty$	$c_{con} \to$ (or $c_{con} \to c_{con,\ bulk}$)
Continuous phase around droplet ('*outer annulus*')	IC	$t = 0$	$r_d \leqslant R_d$	$c_{con} = 0$ (or $c_{con} = c_{con,bulk}$)
	BC	$t > 0$	$r_d = R_d$	$c_{dis} = c_{con} m_R$
				$J_{con} = J_{dis}$
Dispersed phase ('*inner annulus*')	IC	$t = 0$	$r_d \leqslant R_d$	$c_{dis} = 0$ (or $c_{dis} = c_{dis,bulk}$)
	BC	$t > 0$	$r_d = R_d$	$c_{dis} = c_{con} m_R$
				$J_{con} = J_{dis}$
Dispersed phase ('*inner square*')	IC	$t = 0$	$x \geqslant 0$	$c_{dis} = 0$

[a]The center of the coordinate system is placed at the center of the droplet.
[b]The center of the coordinate system is placed at the center of the gas bubble.
[c]No boundary conditions are required at the overlap-boundaries: '*outer annulus*'/'*Background*' and '*inner square*'/'*inner annulus*'. The boundary condition at the droplet surface $r_d = R_d$ is defined in Eqs. (1a) and (1b)

Table 5
Input parameters

Independent parameter values		Depending parameter values	
k_L	1.16×10^{-4} (m/s)	τ	0.117332 (s)
D_c	1.24×10^{-9} (m^2/s)	d_p	42.76×10^{-6} (m)
D_d	2.30×10^{-9} (m^2/s)	D_R	1.85 (−)
m_R	103 (−)		
d_p	3×10^{-6} (m)[a]		

[a] Littel et al. (1994) mentioned that "the dispersed phase droplets were smaller than 3 μm."

coefficient (not shown in the figures). The distance of the droplet to the gas–liquid interface seems to have no significant influence on the foreland area (Fig. 9a), however, the enhancement factors obtained increase strongly with decreasing distance of the droplet to the gas–liquid interface. This latter result was also found for the 1-D model (see Brilman et al., 1998).

The importance of the radius of the foreland was further analyzed with the aid of Figs. 10a and b. In Fig. 10a the local enhancement factors $E(y, \tau)$ at different radial positions from the projected center of the particle on the gas–liquid interface as well as the corresponding interfacial area are represented for a 3-D simulation. In Fig. 10b these are combined to yield the relative contribution to the additional flux due to the presence of the droplet for every radial position. Note that for a 2-D calculation a similar representation can be constructed, but in these cases the differences in fractional surface 'area' (*line pieces*) of the gas–liquid interface, will be less pronounced.

In Fig. 10b it can be recognized that only about 1/3 of the additional gas-phase component absorbed is accounted for in the area covered by the projection of the droplet on the gas–liquid interface, and thus 2/3 of the additional absorption occurs in the foreland outside this projection area.

The total amount of gas-phase component which will be absorbed in addition to the amount absorbed by an

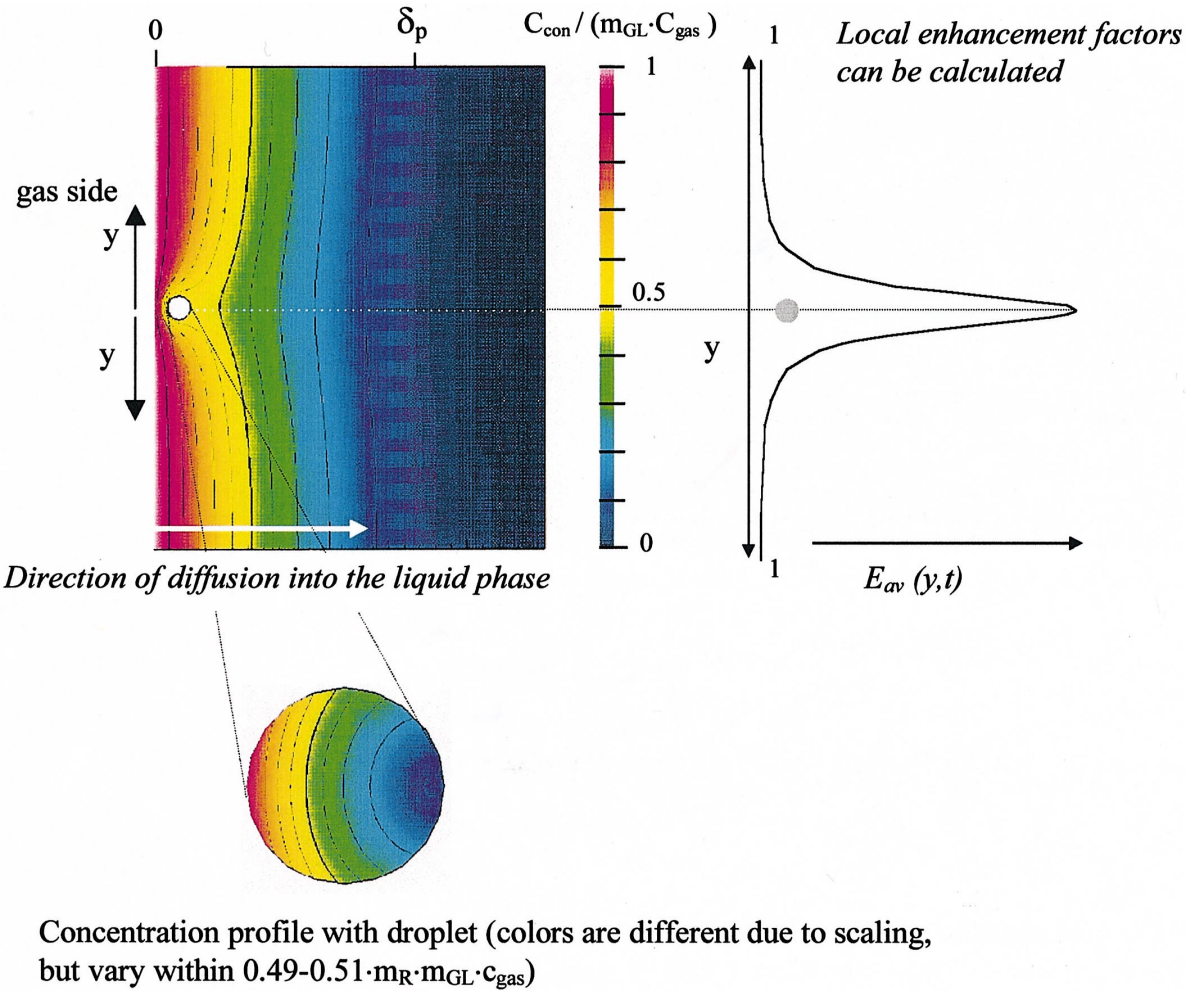

Fig. 8. Typical simulation results: a concentration field around the droplet and the local enhancement factors, evaluated at the gas–liquid interface.

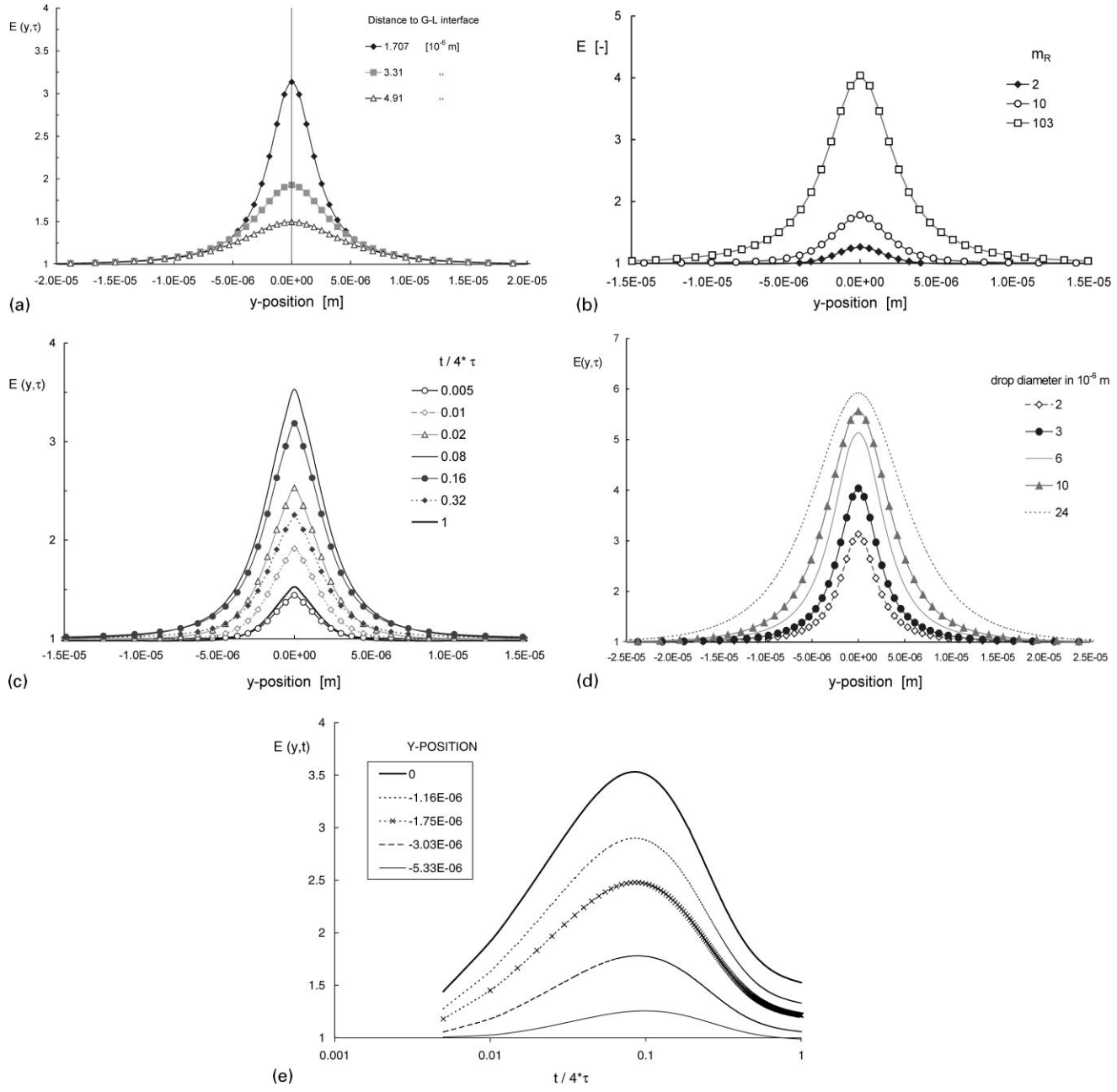

Fig. 9. Some typical (2-D) single particle simulation results showing the effects of several parameters (default values are given in Table 5 and default L value = 1.7 mm). a. Effect of distance to gas–liquid interface (L). b. Variation of relative solubility m_R. c. $E(y)$ at different contact times $0 \leqslant t \leqslant 4\tau$. d. Variation of droplet diameter. e. $E(t)$ for $0 \leqslant t \leqslant 4\tau$ for 5 y-positions.

equivalent liquid-phase package without a droplet can be calculated by integrating the additional flux (which is equal to: $J_{\mathrm{ph}} \cdot (E(y, t) - 1)$) over the foreland area. It was found that the total amount of gas-phase component absorbed in the dispersed phase droplet exceeds the *additional* amount absorbed through the gas–liquid interface. In other words, the droplet acts as a sink for the diffusing gas-phase component due to the local distribution of the gas-phase component.

4. Particle–particle interaction

Another important feature is that the presence of other particles in the vicinity of the particle considered may affect its influence on the gas absorption. In this section it is investigated how the presence of additional particles influences the overall absorption flux. In these simulations the default physico-chemical parameter values are taken equal to those presented in Table 5,

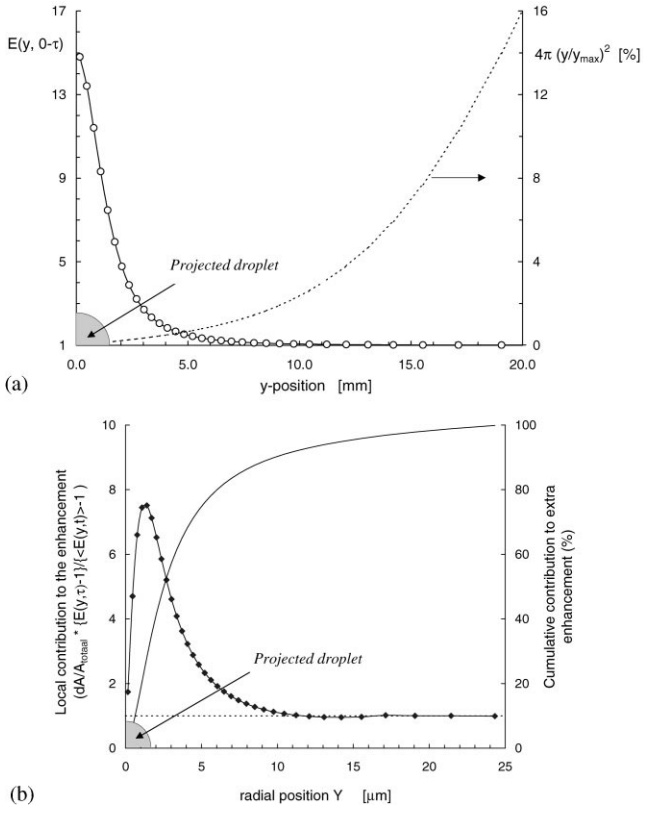

Fig. 10. Analysis of the contribution to mass transfer enhancement at different radial positions. a. Local enhancement factors at different y-positions. b. Contribution to mass transfer enhancement at different radial positions.

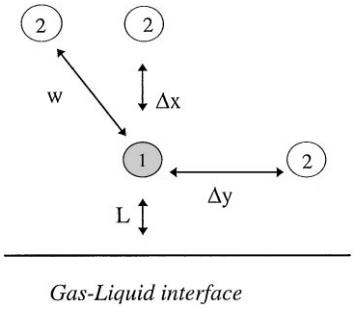

Fig. 11. Two particle configurations.

only the number of particles and their position is varied.

Interaction between the enhancing effect of particles occurs when the total effect of the particles differs from the sum of the individual contributions of the separate particles if no other particles were present. This interaction is studied for several particle configurations, using the two-dimensional model. First, interactions between two particles were considered as schemetically shown in Fig. 11.

Some results of these simulations are shown in Fig. 12. In these figures the calculated local enhancement curve for the two particle configuration as well as the individual contributions of the particles respectively and the summation of the their contributions is presented. For particles located directly behind each other (with respect to the interface, see Fig. 12c) it is found that the particles located directly behind the first one contribute marginally to the mass transfer enhancement. This is not only due to the larger distance to the interface for the second particle, but mainly to the shielding effect by the first particle.

As it may be expected, the interaction (in fact the deviation between the two particle simulation and the sum of both single particle contributions) increases with decreasing distance between the particles considered. For three particle simulations similar results were found, see Figs. 13a–d.

The interaction may be quantified by defining an interaction factor I as the ratio of the actual enhancement factor to the summation of the contributions of the particles separately;

$$I(y) = \frac{\sum_{i=1}^{N} E(y) - (N-1)}{E_{N\text{particles}}(y)}. \tag{3}$$

The value found for this interaction factor will vary with the y-position along the gas–liquid interface. For the simulation case of Table 5, the interaction factor I decreases strongly (and thus interaction becomes increasingly important) at interparticle distances below 5 μm. At interparticle distances exceeding 5 μm the particle–particle interaction may be neglected (deviations less than 3%). For other sets of physico-chemical parameters the mentioned threshold value of 5 μm will be different, e.g. for larger values of D_{con} the threshold value will be higher.

Since the number of multi-particle configurations possible is infinite, it would be advantageous if the enhancement factors for a specific multi-particle configuration could be described on beforehand from the results for single particle simulations. It was found that the calculated local enhancement factors for the two- and three-particle curves can be described satisfactory accurate well using the following correlation, in which all binary particle–particle interactions are accounted for:

$$E_{N_{\text{particles}}}(y) = \sum_{i=1}^{N} E_i(y) - \frac{(N-1)}{1/2N(N-1)} \times \left(\sum_{i=1}^{N-1} \sum_{\substack{j=i+1 \\ i \neq j}}^{N} (E_i(y)E_j(y))^{C(w_{i\to j})} \right). \tag{4}$$

In this correlation the only remaining (fit)-parameter is C, which is a function of the interparticle distance (surface to surface) $\Delta w_{i\to j}$. For the parameter set of

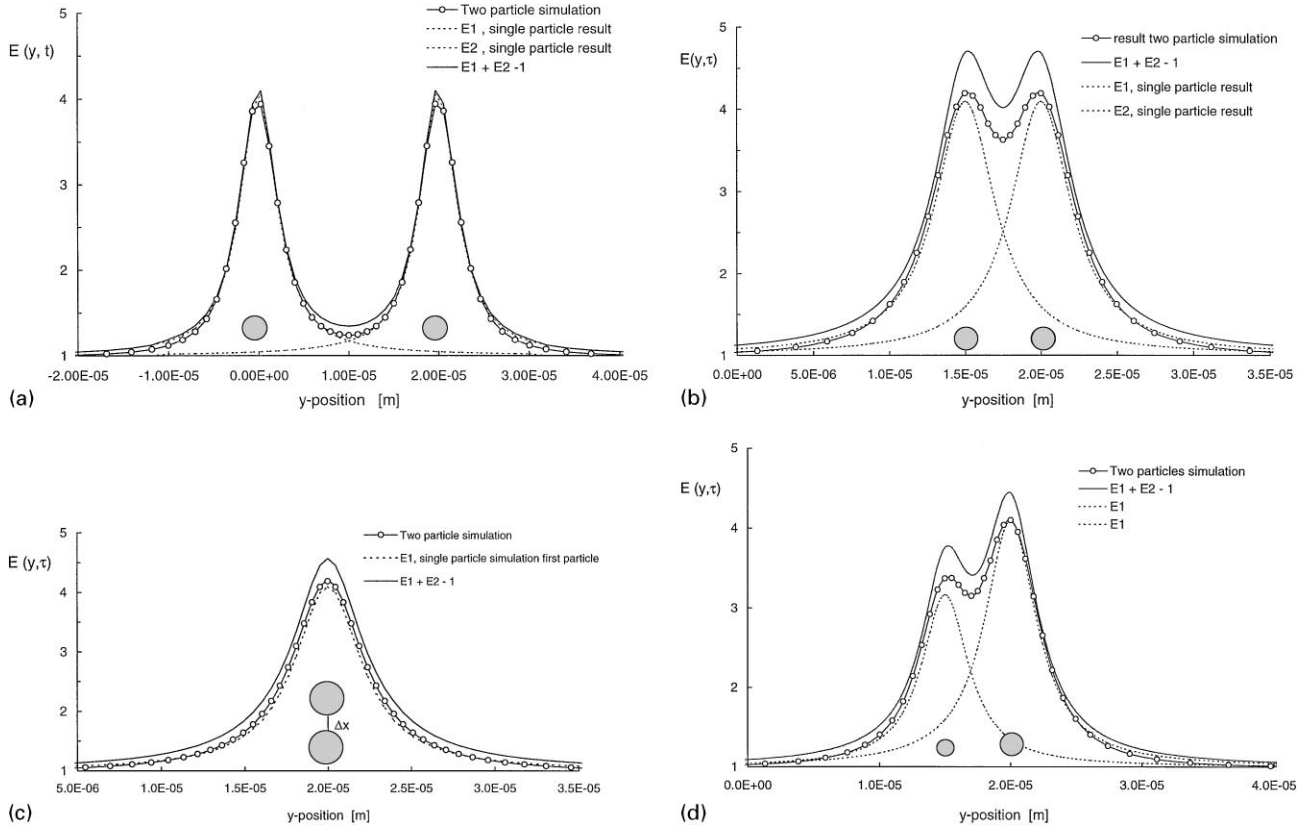

Fig. 12. a. 2-D simulations for two particles an interparticle distance of 17 μm. b. 2-D simulations for two particles an interparticle distance of 2 μm. c. 2-D simulations for two particles directly behind each other. d. 2-D simulations for a 2 μm and a 3 μm particle located at the same distance to the G–L interface.

Table 5 the correlation of C with w is found to be:

$$w \leqslant 5\ \mu\text{m} \quad C = 0.1 + (5.0 \cdot 10^{-6} - w_{i\to j})0.05/w_{i\to j} \quad (w_{i\to j} \text{in } [\mu\text{m}])$$

$$w > 5\ \mu\text{m} \quad C = 0.1$$

For the considered set of parameter values, this particle interaction description was tested for a 5 particle configuration. The results are given in Fig. 14. From these results it is concluded that the $E(y, \tau)$ profile is predicted reasonably accurate from the single particle simulations.

5. On the prediction of absorption fluxes

For calculating the overall gas absorption fluxes into emulsions or liquid–liquid dispersions using a heterogeneous model all the possible particle configurations at the interfaces must be taken into account and the enhancement factors for these situations should be calculated. Alternatively, an unit cell may be defined in which the particle configuration is such that the absorption flux for this unit cell represents the average absorption flux for the particular system and all interactions are corrected for. Holstvoogd et al. (1988) arbitrarily choose to place one particle in the center of a unit, cubic, cell (see Table 3). Karve and Juvekar (1990) took a cylindrical unit cell with one particle (see Table 3). However, this unit cell, implemented with a symmetry boundary at the cylindrical wall overestimates the dispersed phase holdup surrounding this unit cell, owing to the cylindrical geometry. The same holds for the work of Lin, Zhou and Xu (1999).

Single particle calculations have shown that especially those particles located most closely to the interface contribute to the mass transfer enhancement. In multiparticle simulations the mass transfer enhancement depends on the position of the particles with respect to each other and to the gas–liquid interface. The interaction algorithm, taking the binary particle–particle interaction pairs into account, was found to describe reasonably well the local enhancement factors for the 2-D cases considered. With this, the effect of interaction of different particle configurations can now be evaluated. Since it is impossible to evaluate every possible configuration, the sensitivity of the average absorption flux in a multiparticle cell to the particle configuration is studied. From

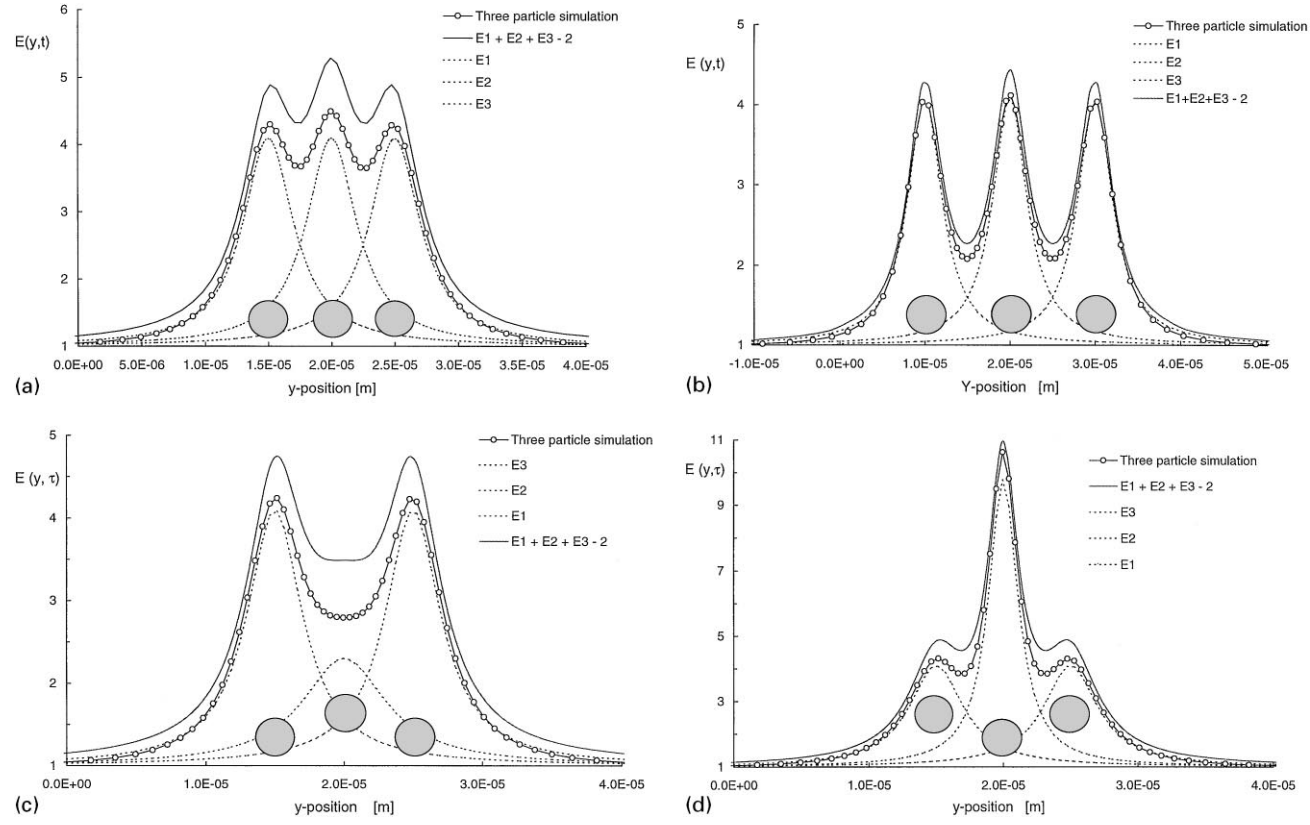

Fig. 13. a. Three identical particles at equal distance from the gas–liquid interface and an interparticle distance of 2 μm. b. Three particles, at equal distance from the G–L interface. Interparticle distance: 7 μm. c. Three particles, the outer particles are located more close to the gas–liquid interface. d. Three particles, the middle one is located closer to the gas–liquid interface.

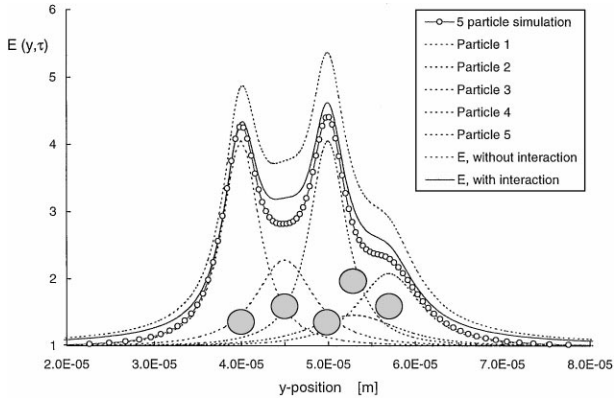

Fig. 14. Five particle simulation; testing the interaction correlation.

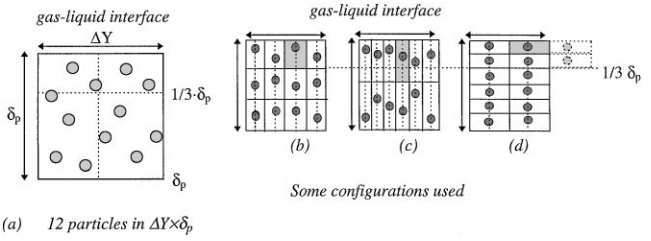

Fig. 15. Some particle configurations used in the sensitivity study.

this it might be ultimately possible to arrive at a representative unit cell configuration.

For this purpose a multi-particle cell was defined, with 12 particles present in a certain area in combination with various combinations. The area was chosen such that the holdup (by surface for the 2-D model) was equal to 3.4%. The area $\delta_p \times \Delta Y$ was divided (in 6 different ways) in 12 equally sized rectangular single particle cells, which, on the average, will contain one single particle each (so-called 'single particle cells'). Examples of these subdivisions are given in Fig. 15.

For these configurations one single particle cell located at the gas–liquid interface was considered and the local enhancement curves $E(L, y, \tau)$ were integrated and averaged over all possible particle positions within the cell, on the centerline perpendicular to the gas–liquid interface, to yield $\bar{E}_L(y, \tau)$. To allow analytical integration, the $E(L, y, \tau)$ curves were fitted (without significant loss in accuracy) using a Cauchy distribution function

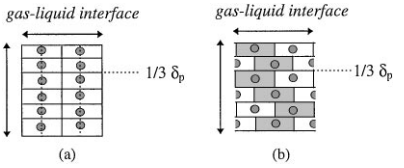

Fig. 16. Shifted half-a-cell position aside to avoid the maximum shielding effect.

$E(L, y, \tau) = 1 + A/(1 + (y/B)^2)$ in which the parameters A and B depend only on L.

$$\overline{E_L}(y, \tau) = \frac{\int_{L=0}^{L=d_{spc}-1/2d_p} E(L, y, \tau)\mathrm{d}L}{\int_{L=0}^{L=d_{spc}-1/2d_p} \mathrm{d}L}. \quad (5)$$

In the next step, the interaction between particles in adjacent cells was taken into account via Eq. (4), using the L-averaged enhancement relations from Eq. (5). By doing so, it is assumed that the interaction of the $\overline{E_L}(y, \tau)$ curves for the separate particles is a good approach to averaging over all possible configurations, each with its own interaction characteristics. This assumption was supported by test calculations with three adjacent cells. In each of these cells 20 particle positions on the centerline were chosen. The average $E(y, \tau)$ relation for these $20 \times 20 \times 20$ situations was found to be equal to the $\overline{E(y, \tau)}$ relation obtained by the interaction of the three $\overline{E_L}(y, \tau)$ relations. In another test the assumption of locating all particles at the centerline of their respective single

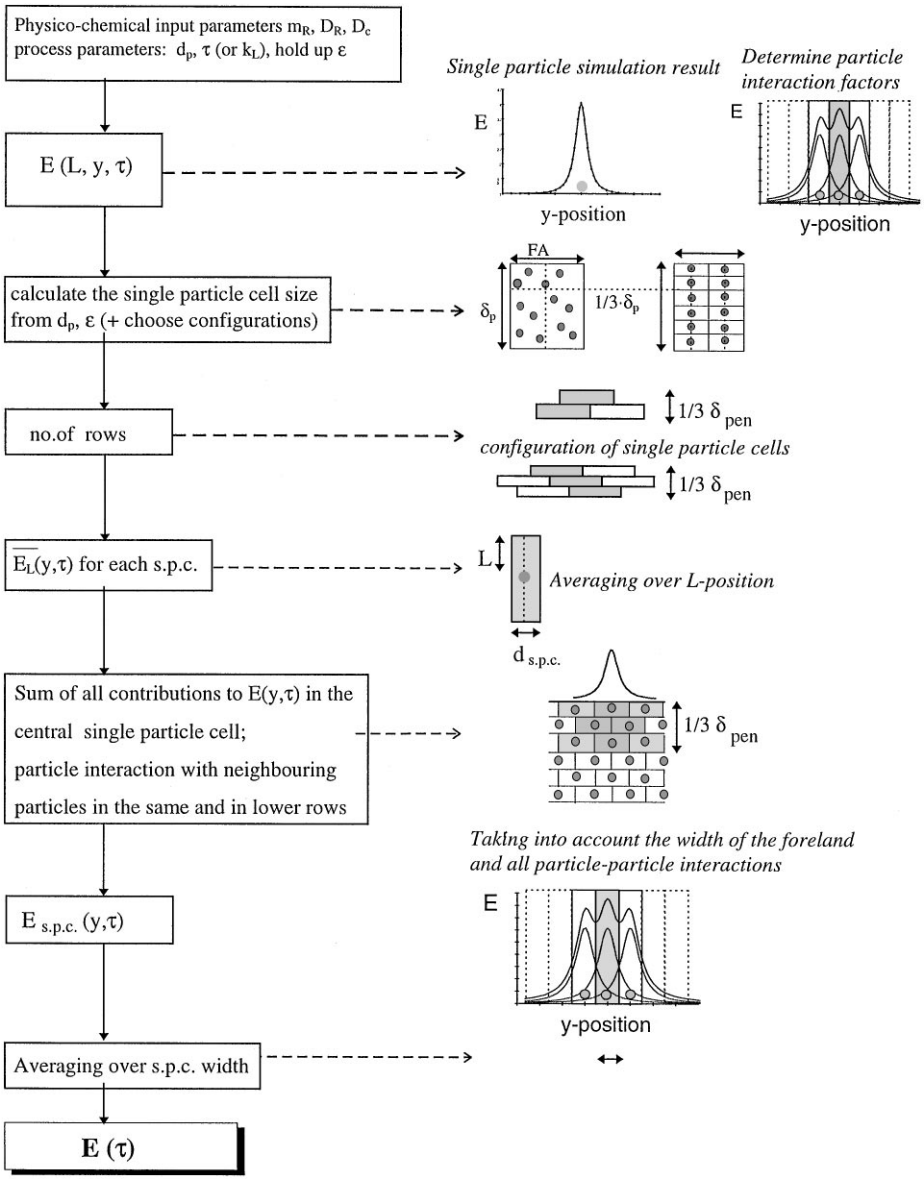

Fig. 17. Procedure for calculating the average enhancement factor from heterogeneous, single particle models {spc = single particle cell}.

Table 6
Effect of single particle cell configuration

Configuration	$E_{av,cell}$ (3 μm)	$E_{av,cell}$ (2 μm)	
1×12	1.73	2.14	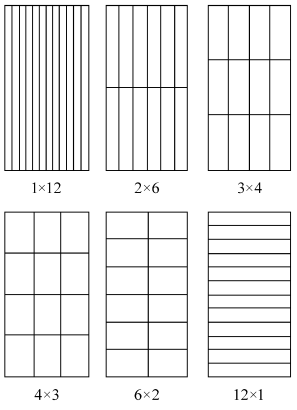
2×6	1.71	2.09	
3×4	1.72	2.05	
4×3	1.76	2.10	
6×2	1.77	2.10	
12×1	1.88	2.15	

particle cell was tested by allowing 45 positions (3 lines $\times 15$ positions per line) *per* cell, again for three adjacent cells. All tests showed that these assumptions cause little error ($< 5\%$).

Single particle simulations have shown that droplets located at $L > 1/3\delta_p$ have no significant influence on the flux enhancement, see also Brilman et al. (1998). Therefore, for those configurations where the depth of the single particle cell exceeds this value, the cells behind the cell adjacent to the gas–liquid interface were neglected. However, this is not the case for configurations like in Fig. 15d, where also the second row of single particle cells will contribute to the mass transfer enhancement. However, a maximum shielding effect is obtained if the particles are located directly behind one another, as will be clear from Fig. 12c. To avoid this, the second row is shifted half-a-cell position aside. This is represented in Fig. 16. When N rows should be taken into account, each row is shifted (1/N)th part aside. After this, the contribution of the second row of cells, taking into account the interaction terms, was also included. The 2-D single particle results (for 3 μm and for 2 μm droplets) were used to evaluate the different single particle cell configurations, see Table 6.

From these results it is concluded that the configuration of the unit cell does not influence significantly the overall enhancement factor calculated, if the configuration of the single particle cell is chosen not too extreme. In Fig. 17 the complete procedure for flux prediction from single particle simulations using particle-particle interaction is represented.

This procedure is used to evaluate the average enhancement factor using the 3-D simulations for the parameter set of Table 5, representing the measurements of Littel et al. (1994). Using these 3-D single particle simulations and the strategy proposed in Fig. 17 the results of Fig. 18 were obtained.

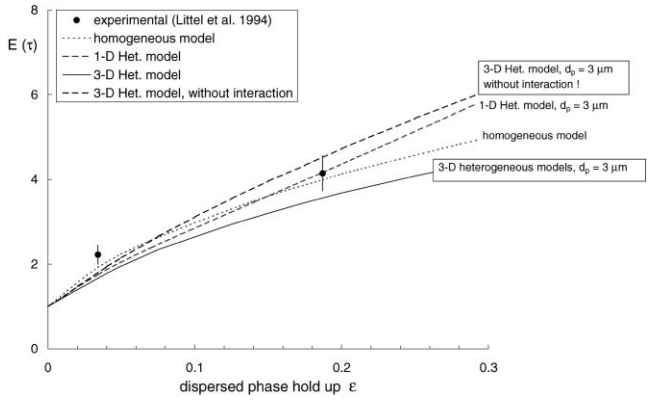

Fig. 18. Comparison of results obtained with the 1-D and 3-D instationary heterogeneous models with a homogeneous model and experimental data by Littel et al. (1994).

It can be seen from the results of the 3-D heterogeneous model that inclusion of the particle interaction leads to a more logarithmic shape of the E–ε curve, which is also predicted by the homogeneous models and observed in other experimental studies (see Fig. 1). This was not found for the 1-D model, because in the latter model particle interaction is negligible (all particles lie behind one another) and an increase in the dispersed phase holdup only leads to a smaller distancer of the first particle to the gas–liquid interface. Although the results of the much simpler homogeneous model are reasonably good in this case, it must be realized that the physical nature of that model is not correct, and this might lead to unreliable modelpredictions in more complicated situations.

The simulation results of the 3-D heterogeneous model for the data by Littel et al. (1994) show an underprediction of the mass transfer enhancement when assuming a droplet size of 3 μm. For a slightly smaller droplet size a better description would have been obtained (see also Table 6). The average droplet size in the experiments might have been less than the 3 μm used in the simulations. However, since the exact average dropsize (and size distribution) is not known, no further validation is possible.

The 3-D simulation data presented in Fig. 18 were calculated for different numbers of rows and for different aspect ratios of the unit cell. The latter effect was negligible, but the number of rows had a minor influence ($< 5\%$) at higher holdups. This is believed to be caused by the limitations of the fit of the simulation data at small distances to the gas–liquid interface. More single particle simulations under these conditions could resolve this influence.

6. Discussion and conclusions

Heterogeneous mass transfer models have been developed to study the effect of particles near the gas–liquid

interface on the gas-absorption rate. Using the developed models the relative importance of particle capacity parameters and particle position are now clear from single particle simulations. Particle interaction was studied extensively for the 2-D models, and to a lesser extent for the 3-D models. An interaction algorithm valid for the specific set of parameters considered (Table 5) was identified and gave good results in predicting the absorption fluxes for multi-particle simulations. However, for other sets of physico-chemical parameters the (coefficients used in the) algorithm should be determined again by fitting another set of simulations (multi particle simulations or 2-D single particle simulations using symmetry at the boundaries of the single particle cell). Taking all particle interactions into account, the shape of the single particle cell (the size is already determined by the holdup) can be chosen rather arbitrarily. A procedure for predicting the absorption flux for gas absorption in heterogeneous media has been proposed in Fig. 17.

From the results of Fig. 18 for the variation of the enhancement factor at increasing holdup, it is clear that particle–particle interaction should be taken into account in the heterogeneous models in order to be able to describe the enhancement factor leveling off at higher holdups. Note, that at higher holdups also other hydrodynamic parameters (like the characteristic surface renewal time) may have changed in the experiments and even direct gas-dispersed liquid phase contact may become important.

The results obtained using the models developed and the strategy proposed seem to follow the general experimental trends and described reasonably well the data by Littel et al. (1994). However, accurate comparison is difficult since no accurate data on dispersed phase droplet size and distribution were reported. Further validation of the model is desired and awaiting new, accurately defined experiments.

Acknowledgements

The authors wish to acknowledge W.D. Henshaw (Los Alamos Nat. Lab., USA) for providing the Overture Overlapping Grid software and S. Maas for her contribution to the development, and application of the models.

References

Alper, E., & Deckwer, W. D. (1981). Comments on gas absorption with catalytic reaction. *Chemical Engineering Science*, *36*, 1097–1099.

Alper, E., Wichtendahl, B., & Deckwer, W. D. (1980). Gas absorption mechanism in catalytic slurry reactors. *Chemical Engineering Science*, *35*, 217–222.

Beenackers, A. A. C. M., & van Swaaij, W. P. M. (1993). Mass transfer in gas–liquid slurry reactors. *Chemical Engineering Science*, *48*, 3109–3139.

Brilman, D. W. F., van Swaaij, W. P. M., & Versteeg, G. F. (1998). A one-dimensional instationary heterogeneous mass transfer model for gas absorption in multiphase systems. *Chemical Engineering & Processing*, *37*, 471–488.

Bruining, W. J., Joosten, G. E. H., Beenackers, A. A. C. M., & Hofman, H. (1986). Enhancement of gas–liquid mass transfer by a dispersed second liquid phase. *Chemical Engineering Science*, *41*, 1873–1877.

Chesshire, G., & Henshaw, W. D. (1994). Composite overlapping meshes for the solution of partial differential equations. *Journal of Computational Physics*, *90*, 1–64.

Ede, C. J. van, Van Houten, R., & Beenackers, A. A. C. M. (1995). Enhancement of gas to water mass transfer rates by a dispersed organic phase. *Chemical Engineering Science*, *50*, 2911–2922.

Holstvoogd, R. D., van Swaaij, W. P. M., & Dierendonck, L. L. van (1988). The absorption of gases in aqueous activated carbon slurries enhanced by adsorbing or catalytic particles. *Chemical Engineering Science*, *43*, 2182–2187.

Junker, B. H., Wang, D. I. C., & Hatton, A. H. (1990a). Oxygen transfer enhancement in aqueous/perfluorocarbon fermentation systems: I. Experimental observations. *Biotechnology and Bioengineering*, *35*, 578–585.

Junker, B. H., Wang, D. I. C., & Hatton, A. H. (1990b). Oxygen transfer enhancement in aqueous/perfluorocarbon fermentation systems: II. Theoretical analysis. *Biotechnology and Bioengineering*, *35*, 586–597.

Kars, R. L., Best, R. J., & Drinkenburg, A. A. H. (1979). The sorption of propane in slurries of active carbon in water. *Chemical Engineering Journal*, *17*, 201–210.

Karve, S., & Juvekar, V. A. (1990). Gas absorption into slurries containing fine catalyst particles. *Chemical Engineering Science*, *45*, 587–594.

Lin, C., Zhou, M., & Xu, C. J. (1999). Axisymmetrical two-dimensional heterogeneous mass transfer model for the absorption of gas into liquid–liquid dispersions. *Chemical Engineering Science*, *54*, 389–399.

Littel, R. J., Versteeg, G. F., & van Swaaij, W. P. M. (1994). Physical absorption of CO_2 and propene into toluene/water emulsions. *A. I. Ch. E. Journal*, *40*, 1629–1638.

Meer, A. B. van der, Beenackers, A. A. C. M., Burghard, R., Mulder, N. H., & Fok, J. J. (1992). Gas/liquid mass transfer in a four-phase stirred fermentator: Effects of organic phase hold-up and concentration. *Chemical Engineering Science*, 47, 2369–2374.

Mehra, A. (1988). Intensification of multiphase reactions through the use of a microphase-I. Theoretical. *Chemical Engineering Science*, *43*, 899–912.

Mehra, A., Pandit, A., & Sharma, M. M. (1988). Intensification of multiphase reactions through the use of a microphase-II. Experimental. *Chemical Engineering Science*, *43*, 913–927.

Mehra, A., & Sharma, M. M. (1985). Absorption with reaction: Effect of emulsified liquid phase. *Chemical Engineering Science*, *40*, 2382–2385.

Nagy, E. (1995). Three-phase mass transfer: one dimensional heterogeneous model. *Chemical Engineering Science*, *50*, 827–836.

Nagy, E., & Moser, A. (1995). Three-phase mass transfer: Improved pseudo-homogeneous model. *A. I. Ch. E. Journal*, *41*, 23–34.

Nishikawa, M., Kayama, T., Nishioka, S., & Nishikawa, S. (1994). Drop size distribution in mixing vessel with aeration. *Chemical Engineering Science, 49*, 2379–2384.

Pal, S. K., Sharma, M. M., & Juvekar, V. A. (1982). Fast reactions in slurry reactors: Catalyst particle size smaller than film thickness: Oxidation of aqueous sodium sulphide solutions with activated carbon particles as catalyst at elevated temperatures. *Chemical Engineering Science*, *37*, 327–336.

Rols, J. L., Condoret, J. S., Fonade, C., & Goma, G. (1990). Mechanism of enhanced oxygen transfer in fermentation using emulsified oxygen-vectors. *Biotechnology and Bioengineering*, *35*, 427–435.

Rols, J. L., Condoret, J. S., Fonade, C., & Goma, G. (1991). Modeling of oxygen transfer in water through emulsified organic liquids. *Chemical Engineering Science*, *46*, 1869–1873.

Saraph, V. S., & Mehra, A. (1994). Microphase autocatalysis: importance of near interface effects. *Chemical Engineering Science*, *49*, 949–956.

TableCurve version1.0, Jandel Scientific.

Tinge, J. T., & Drinkenburg, A. A. H. (1995). The enhancement of the physical absorption of gases in aqueous activated carbon slurries. *Chemical Engineering Science*, *50*, 937–942.

Tinge, J. T., Mencke, K., & Drinkenburg, A. A. H. (1987). The absorption of propane and ethene in slurries of activated carbon in water-I. *Chemical Engineering Science*, *42*, 1899–1907.

Venugopal, B. V., & Mehra, A. (1994). Gas absorption accompanied by fast chemical reaction in water-in-oil emulsions. *Chemical Engineering Science*, *49*, 3331–3336.

Vinke, H. (1992). *The effect of catalyst particle to bubble adhesion on the mass transfer in agitated slurry reactors*, Ph.D. thesis, Municipal University of Amsterdam, The Netherlands.